Thermal dependence of the zero-bias conductance through a nanostructure

A. C. Seridonio[1,2], M. Yoshida[3] and L. N. Oliveira[1]

[1] *Departamento de Física e Informática, Instituto de Física de São Carlos, Universidade de São Paulo, 369, São Carlos, SP, Brazil*
[2] *ICCMP - International Center for Condensed Matter Physics, Universidade de Brasília, 04513, Brasília, DF, Brazil*
[3] *Departamento de Física, Instituto de Geociências e Ciências Exatas, Universidade Estadual Paulista, 13500, Rio Claro, SP, Brazil*

PACS 73.23.-b – Electronic transport in mesoscopic systems
PACS 73.21.La – Quantum dots
PACS 72.15.Qm – Scattering mechanisms and Kondo effect
PACS 73.23.Hk – Coulomb blockade; single-electron tunneling

Abstract. - We show that the conductance of a quantum wire side-coupled to a quantum dot, with a gate potential favoring the formation of a dot magnetic moment, is a universal function of the temperature. Universality prevails even if the currents through the dot and the wire interfere. We apply this result to the experimental data of Sato et al. [Phys. Rev. Lett. **95**, 066801 (2005)].

Nanodevices owe much of their development to the theory of many-body phenomena. Consider, e. g., the *single electron transistor* (SET), a quantum dot bridging two otherwise independent two-dimensional electron gases [1,2]. The competition between the Coulomb blockade, which bars transport through the dot, and the Kondo screening of the dot magnetic moment by the electron gases [3], which favors low-temperature conduction, was discussed on blackboards [4] a decade before it surfaced in the laboratory [1]. By the time the first device was developed, quantitatively accurate theoretical results were available. Chiefly important was the universal conductance curve $G^S_{SET}(T)$ for the symmetric Anderson model [5,6], which was shown to match the temperature dependence of the zero-bias conductances in SETs and analogous devices.

More recently, experiment has leaped ahead of theory. The development of complex structures, such as the *side-coupled* device [7–12], has motivated only qualitative predictions. As Fig. 1 shows, the current in the side-coupled device is carried by electrons that can either traverse the quantum wire or hop to a quantum dot to skip the central section [12]. A Fano parameter q [13], defined below, measures the amplitude for the latter process relative to that for the former. The limit $q \to \infty$ emulates a SET. For smaller q's, the wire bypasses the Coulomb blockade and allows high-temperature conduction. Below the Kondo temperature T_K, the screening of the magnetic moment enhances the electronic flux through the dot and allows interference with the flow along the central portion of the wire [14,15].

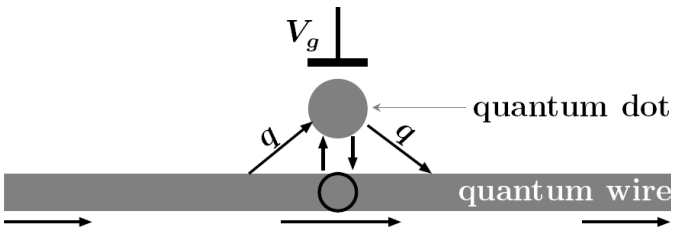

Figure 1: Side-coupled device. The gate potential V_g controls the energy ε_d of the quantum-dot level c_d. The open circle depicts the Wannier orbital f_0.

Attentive to the diversity of experimental findings, we have applied numerical renormalization-group (NRG) tools to an Anderson Hamiltonian modeling the side-coupled device. The resulting essentially exact numerical data for the temperature-dependent conductance $G_q(T)$ will be detailed elsewhere [16]. Here, we focus the relation between $G_q(T)$ and the universal curve $G^S_{SET}(T)$. Our central result covers the Kondo domain, the set of dot energies and dot-wire couplings that favor the formation of

a Kondo screening cloud.

Since the thermodynamical properties of the Kondo crossover are universal functions of the temperature scaled by T_K [2, 17–25], a mathematical relation between $G_q(T/T_K)$ and the universal function $G^S_{SET}(T/T_K)$ is hardly surprising. Nonetheless, the diversity manifest in conductances that, in contrast with $G^S_{SET}(T)$, rise with temperature and in conductance profiles (fixed-T conductance-vs. gate-voltage plots) that display antiresonances [12] rules out a proportionality between $G_q(T)$ and $G^S_{SET}(T)$. Instead, we will show that a linear mapping binds the two functions:

$$G_q(\frac{T}{T_K}) - \frac{\mathcal{G}_2}{2} = \left(G^S_{SET}(\frac{T}{T_K}) - \frac{\mathcal{G}_2}{2} \right) \cos 2\delta, \qquad (1)$$

where δ is the ground-state phase shift of the wire electrons, and $\mathcal{G}_2 \equiv 2e^2/h$, the quantum conductance.

While the mapping (1) is universal, the phase shift and Kondo temperature are model-parameter dependent. At fixed temperature, the Fano parameter q controls the functional dependence of the conductance on the gate voltage V_g. As q grows, valleys in the conductance profiles evolve into plateaus, a result in qualitative agreement with measurements. Most importantly, Eq. (1) affords quantitative comparison with experiment; as an illustration, we will present curves that reproduce the temperature-dependent conductances reported by Sato et al. [8]; show that the dot moment was fully screened; and extract T_K and δ from the data. Our results justify mathematically the authors' phenomenological treatment of their results.

Overview. Preliminary to the formalism, we present an overview of conduction in the side-coupled device. We consider weak coupling to the wire, so that the dot occupation n_d is nearly conserved, and illustrate the discussion with NRG plots of the temperature-dependent conductance.

The device has three characteristic energy scales, set by (i) the coupling to the wire, which broadens the dot levels; (ii) the electrostatic barrier Δ_N between adjacent dot occupations $n_d = N - 1$ and $n_d = N$; and (iii) the Kondo temperature T_K, below which the wire electrons screen the dot moment. The first two scales catch the eye in conductance profiles. The third one defines the thermal regimes $T \gg T_K$ and $T \ll T_K$ displayed schematically in the top and bottom panels of Fig. 2a, respectively.

Left: $q \gg 1$. If $T \gg T_K$ (top), the Coulomb blockade impedes conduction; to defeat it, the gate voltage must be raised, so that the $n_d = N$ and the $n_d = N + 1$ ground states are nearly degenerate. The conductance profile is hence a sequence of narrow resonances. Upon cooling (bottom), little changes if V_g makes n_d even. For odd n_d, however, the Kondo hybridization between the wire and the dot states allows conduction. The conductance $G(V_g)$ alternates between insulating valleys ($G = 0$ for even n_d) and *Kondo plateaus* ($G = \mathcal{G}_2$ for odd n_d) [27].

Right: $q = 0$. The pattern is reversed. If $T \gg T_K$ (top), except at the resonant voltages, the flux through the wire is ballistic. On resonance, the strong coupling to the dot blocks conduction, and $G(V_g)$ dips to zero [28]. For $T \ll T_K$ (bottom) and odd n_d, the screening cloud blocks the wire. The conductance thus alternates between ballistic plateaus and *Kondo valleys* [14].

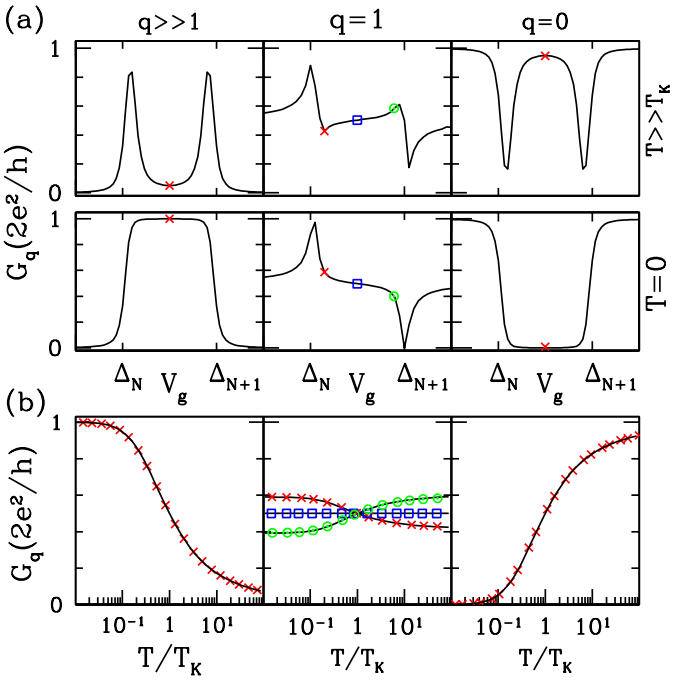

Figure 2: Bird's eye view of conduction through the side-coupled device. (a) Condutance G as a function of applied gate voltage for three representative Fano parameters q at temperatures high (top panels) or low in comparison with the Kondo temperature T_K. (b) NRG results for $G(T)$. The crosses, squares, and circles in each panel represent conductances calculated at the voltages indicated by the same symbol in the panels directly above it. The solid lines depict Eq. (1), with δ extracted from the low-energy fixed-point eigenvalues [26].

Center: $q = 1$. There are now two conduction paths. If $T \gg T_K$ (top), Fano antiresonances near the resonant voltages signal interference between the two currents. Off resonance, the electrons flow only through the wire, and the conductance remains close to $\mathcal{G}_2/2$. For $T \ll T_K$ (bottom) and odd n_d, again the Kondo hybridization to the wire allows conduction through the dot. The Kondo cloud nonetheless blocks conduction through the wire, so that the off-resonance conductance is again close to $\mathcal{G}_2/2$.

For each voltage identified by two crosses, squares, or circles in Fig. 2a, Fig. 2b displays our NRG results for the conductance as a function of T normalized by T_K—the temperature at which the conductance is half the quantum conductance, $G_q(T = T_K) \equiv \mathcal{G}_2/2$. The agreement with the solid lines representing Eq. (1) is very good: even at the limits of the Kondo regime (crosses and circles, $T = 50\,T_K$) the absolute deviations are smaller than $0.01\,e^2/h$.

For $q \gg 1$ (left, $\delta \approx 0$), the device mimics a SET, the mapping (1) reduces to an identity, and the conduc-

tance decays from ballistic to zero along the universal curve $G^S_{SET}(T)$. The opposite extreme, $q = 0$ (right, $\delta \approx \pi/2$), reverses the pattern: ballistic conductance at $T \gg T_K$, and perfect insulation at $T = 0$. As intuition would dictate, and as general [8] and mathematical [29] arguments suggest, the temperature dependence complements the universal function: $G_q(T) = \mathcal{G}_2 - G^S_{SET}(T)$. For $q \sim 1$ (center, $\delta \approx \pi/4$), three voltages V_g are highlighted. In each case, the conductance interpolates monotonically the high- to the low-temperature limits in Fig. 2a. For $2\varepsilon_d + U = 0$, in particular, Fig. 2a shows that $G_q(T \gg T_K) = G_q(T = 0) = \mathcal{G}_2/2$; the conductance must therefore be constant, $G_q(T) = \mathcal{G}_2/2$, and this is what Eq. (1) predicts for $\delta = \pi/4$.

Model. Hamiltonians describing side-coupled nanostructures, in the geometry of Fig. 1 [12,14,28–30], or other arrangements [31–33] have appeared in print. While our analysis could start from any of the former, to keep the presentation self-contained we define the alternative three-component Hamiltonian $H = H_d + H_w + H_{wd}$. Here, $H_d \equiv \varepsilon_d n_d + U n_{d\uparrow} n_{d\downarrow}$, models the quantum-dot, where $n_d \equiv c^\dagger_d c_d$ is the dot-level occupation; ε_d is the dot energy, controlled by the potential V_g; and U is the Coulomb repulsion. The second term, $H_w \equiv \sum_k \epsilon_k c^\dagger_k c_k + (K/N)\sum_{kk'} c^\dagger_k c_{k'}$, models the wire, of length L. The energies ϵ_k, measured from the Fermi level, form a symmetric, structureless, half-filled conduction band of width $2D$ comprising N levels separated by the splitting $\Delta \equiv 2D/N$ [34]. The scattering K describes the (fixed) gate potential applied to the wire [12].

The last component, $H_{wd} \equiv \sum_k (V_k/\sqrt{N}) c^\dagger_k c_d + \text{H. c.}$, couples the wire to the dot. The relatively small thermal energies $k_B T \ll D$ authorize retention of the two leading terms in the expansion of the coupling V_k in powers of ϵ_k [35]: $V_k \approx V_{k_F} + \epsilon_k (dV/d\epsilon_k)_{k_F}$. We rewrite this approximation as $V_k = V + \pi\rho q V \epsilon_k$, where $\rho \equiv 1/2D$, to define the coupling V and the Fano parameter q [13]. Following NRG tradition, we introduce the shortand $f_0 \equiv \sum_k c_k/\sqrt{N}$. For future reference, we note that, in this notation, the (particle-hole) *symmetric* ($q = K = 2\varepsilon_d + U = 0$) Anderson Hamiltonian reads

$$H^S_0 = \sum_k \epsilon_k c^\dagger_k c_k + V(f^\dagger_0 c_d + \text{H. c.}) - \frac{U}{2}(n_{d\uparrow} - n_{d\downarrow})^2. \quad (2)$$

The conductance is more easily computed on a basis constituted of f_0 and $N-1$ other conduction operators $a_p = \sum_k \alpha_{pk} c_k$, where $p = 2\pi n_p/L$ [$n_p = -N/2+1, \ldots, N/2-1$], such that $\{f^\dagger_0, a_p\} = 0$, and that $\{a^\dagger_p, a_{p'}\} = \delta_{pp'}$ [36]. With the shorthand $f_1 = \sum_p a_p/\sqrt{N-1}$, the model Hamiltonian becomes

$$H_A = \sum_p \tilde{\epsilon}_p a^\dagger_p a_p + K f^\dagger_0 f_0 + (t_0 f^\dagger_1 d_q + V f^\dagger_0 c_d + \text{H. c.}) + H_d, \quad (3)$$

where $\mathcal{N}_q \equiv \sqrt{1 + (\pi\rho V q)^2}$; $\mathcal{N}_q d_q \equiv f_0 + \pi\rho\, q\, V c_d$; $t_0 \equiv D\mathcal{N}_q/\sqrt{3}$; and the energies $\tilde{\epsilon}_k$ are the conduction energies ϵ_k phase shifted by $\pi/2$, i. e., $\tilde{\epsilon}_k \equiv \epsilon_k - \Delta/2$.

If $K \to \infty$, the scattering potential decouples f_0 from the other states, freezes its occupation at $f^\dagger_0 f_0 = 0$, and forces the current through the dot. The condition $2\varepsilon_d + U = 0$ reduces H_A to the *symmetric-SET* Hamiltonian

$$H^S_{SET} = \sum_p \tilde{\epsilon}_p a^\dagger_p a_p + V_q(f^\dagger_1 c_d + \text{H. c.}) - \frac{U}{2}(n_{d\uparrow} - n_{d\downarrow})^2, \quad (4)$$

where $V_q \equiv \pi\, q\, V/(2\sqrt{3})$. Given the analogous definitions $f_0 \sim \sum_k c_k$ and $f_1 \sim \sum_p a_p$, we see that only the phase shifted energies $\tilde{\epsilon}_k = \epsilon_k - \Delta/2$ distinguish H^S_{SET} from H^S_0.

The first term within parentheses on the right-hand side of Eq. (3), which couples the conduction states $f_1 \sim \sum a_p$ to $d_q \sim f_0 + \pi\rho\, q\, V c_d$, is the mathematical expression of the two conduction paths in Fig. 1, one of which runs through the central wire-orbital f_0, and the other, with relative amplitude $\pi\rho\, q\, V$, through the dot orbital c_d. To flow from the left to the right side of the wire, the current must traverse d_q. Accordingly, the Linear-Response Theory [37] shows that ρ_q, the spectral density for the operator d_q, controls the zero-bias conductance:

$$G_q(T) = \mathcal{G}_2 \mathcal{N}_q{}^2 \int_{-D}^{D} \frac{\rho_q(\epsilon, T)}{\rho} \left[-\frac{\partial f(\epsilon)}{\partial \epsilon}\right] \mathrm{d}\epsilon. \quad (5)$$

Here $f(\epsilon)$ is the Fermi function, and

$$\rho_q(\epsilon, T) = \frac{1}{\mathcal{Z}} \sum_{mn} \frac{e^{-\beta E_m}}{f(\epsilon_{mn})} |\langle m|d^\dagger_q|n\rangle|^2 \delta(\epsilon_{mn} - \epsilon), \quad (6)$$

where $\mathcal{Z}$ is the partition function, and $\epsilon_{mn} \equiv E_m - E_n$.

Analysis. We are chiefly interested in the *Kondo regime*, the set of temperatures and model parameters favoring unitary dot occupation, i. e., such that the energies $|\varepsilon_d|$ $(\varepsilon_d + U)$ to remove the dot electron (add a second electron) dwarf the energy $k_B T$ and dot-level width $\Gamma = \pi\rho V^2$. The Kondo temperature T_K then sets the energy scale.

At high temperatures, $T \gg T_K$, the Hamiltonian (3) lies close to an unstable *local-moment* fixed point (LM), which comprises a noninteracting spin-1/2 variable (the dot spin) decoupled from a conduction Hamiltonian [26]

$$H^*_{LM} = \sum_k \epsilon_k c^\dagger_k c_k + K_{LM} f^\dagger_0 f_0, \quad (7)$$

where the effective scattering potential K_{LM} depends on the model parameters. For $H_A = H^S_0$ (H^S_{SET}), in particular, $K_{LM} = 0$ ($K_{LM} \to \infty$).

Diagonalization of the quadratic form (7) yields N eigenoperators g_k and eigenvalues $\varepsilon_k = \epsilon_k - \delta_{LM}\Delta/\pi$:

$$H^*_{LM} = \sum_k \varepsilon_k g^\dagger_k g_k. \quad (8)$$

Near the Fermi level, the phase shifts δ_{LM} are uniform [26].

In analogy with the definitions $f_0 \sim \sum_k c_k$ and $f_1 \sim \sum_k \epsilon_k c_k$, we can define the mutually orthogonal combinations of eigenoperators $\phi_0 = \sum_k g_k/\sqrt{N}$ and $\phi_1 = \sqrt{3/N}\sum_k (\epsilon_k/D) g_k$. For any pair of constants α_0 and α_1,

$$\alpha_0 f_0 + \alpha_1 f_1 = \beta_0 \phi_0 + \beta_1 \phi_1, \quad (9)$$

where β_0 and β_1 are linear combinations of α_0 and α_1, with coefficients fixed by δ_{LM}.

Table 1 collects results for the symmetric [Eq. (2)] and the symmetric-SET [Eq. (4)] Hamiltonians. While columns 3-5 follow from the definitions of g_k, ϕ_0 and ϕ_1, columns 5 and 6 require explanations. For $H_A = H_0^S$ (i. e., $q = K = 2\varepsilon_d + U = 0$), the operator d_q reduces to $f_0 = \phi_0$. Its spectral density $\rho_q \equiv \rho_0^S$ is therefore equal to ρ_{ϕ_0}.

Table 1: Properties of the symmetric Hamiltonians

H_A	δ_{LM}	g_k	ϕ_0	$D\phi_1$	ρ_{ϕ_0}	$\frac{\rho_{\phi_1}}{\mathcal{N}_q{}^2}$
H_0^S	0	c_k	f_0	Df_1	ρ_0^S	
H_{SET}^S	$\pi/2$	a_k	f_1	$\sqrt{\frac{3}{N}}\sum_p \tilde{\epsilon}_p a_p$		ρ_{SET}^S

For $H_A = H_{SET}^S$, d_q reduces $-\pi\rho\, q\, V\, c_d/\mathcal{N}_q$. To relate its spectral density to ρ_{ϕ_1}, choose two eigenstates $|m\rangle$, $|n\rangle$ of H_{SET}^S with $E_m, E_n \approx k_B T \ll D$. In the identity

$$\langle m|\sum_p \frac{[a_p, H_{SET}^S]}{\sqrt{N}}|n\rangle = \frac{D\langle m|\phi_1|n\rangle}{\sqrt{3}} + V_q\langle m|c_d|n\rangle, \quad (10)$$

the left-hand side is then much smaller than each matrix element on the right. This shows that $\langle m|\phi_1|n\rangle \approx -\pi\rho\, q\, V\langle m|c_d|n\rangle$, a result equivalent to $\langle m|\phi_1|n\rangle = -\mathcal{N}_q\langle m|d_q|n\rangle$, and hence to the last column in Table 1.

As the system is cooled, the wire electrons screen the dot moment, and H_A crosses over from the LM to a stable *frozen-level* fixed point (FL). The latter is but the conduction band resulting from letting $K_{LM} \to 1/(\pi^2\rho^2 K_{LM})$ in Eq. (7). Diagonalization of the FL Hamiltonian yields N eigenvalues $\overline{\varepsilon}_k = \epsilon_k - \delta\Delta/\pi$, where, in conformity with Friedel's sum rule [38], the phase shift $\delta = \delta_{LM} - \pi/2$.

Table 2: Conductance at the two fixed points

Fixed point	Phase shift	G_q	G_0^S $(\delta = \pi/2)$	G_{SET}^S $(\delta = 0)$
LM	$\delta + \pi/2$	$\mathcal{G}_2 \sin^2\delta$	$\mathcal{G}_2$	0
FL	δ	$\mathcal{G}_2 \cos^2\delta$	0	$\mathcal{G}_2$

The fixed-point physical properties are independent of temperature and energy. In particular, the LM and FL conductances are trigonometric functions of the phase shift. The expressions, which result from an extension of Langreth's argument [38], are recorded in Table 2.

The effective antiferromagnetic interaction $H_J = J\boldsymbol{S}\cdot\boldsymbol{\sigma}_{\mu\nu}\phi_{0\mu}\phi_{0\nu}$ [18, 26, 39], between the dot spin $\boldsymbol{S}$ and the spin of the localized orbital ϕ_0 drives the Hamiltonian from the LM to the FL. The NRG trajectory is universal: scaled by $k_B T_K$, the eigenvalues of H_A are universal, and so are the corresponding eigenstates on the basis of the $\{g_k\}$ [17, 26, 40]. The spectral densities ρ_{ϕ_0} and ρ_{ϕ_1} in Table 1 are therefore universal functions of the ratios T/T_K and $\epsilon/k_B T_K$. To highlight these findings, we define the scaled energy $\mathcal{E} \equiv \epsilon/k_B T_K$ and temperature $\mathcal{T} \equiv T/T_K$.

Next, we turn to the asymmetric Kondo-domain Hamiltonians. To relate the conductance G_q to the universal function G_{SET}^S, we add to H_A an infinitesimal harmonic perturbation, frequency ω, coupling the spectrum of H_A to an auxiliary orbital $\overline{d}$ at the Fermi level:

$$H_\eta = \eta\, \overline{d}^\dagger d_q\, e^{-i\omega t} + \text{H. c.}. \quad (11)$$

The golden rule shows that the spectral density ρ_q is the response function for the thermally averaged transition rate $j_{\,\overline{d}\to A}$ induced by H_η:

$$\langle j_{\,\overline{d}\to A}(\omega)\rangle_T = (\pi\eta^2/\hbar)\rho_q(\hbar\omega, T). \quad (12)$$

Consider, then, the perturbative effects of H_η upon the Kondo crossover [18]. Close to a (Fermi-liquid) fixed point H^*, that is, for $H = H^* + \delta H$, one can always construct an effective Hamiltonian H_{eff} that reproduces the spectrum of H to linear order in δH. Here, to follow a pedestrian route, we subject the sum $H_A + H_\eta$ to the Schrieffer-Wolff transformation: $H_A^{eff} + H_\eta^{eff} \equiv e^S(H_A + H_\eta)e^{-S}$ [39]. Besides substituting the spin-spin interaction H_J for the dot-wire coupling H_{wd}, this casts Eq. (11) in the form

$$H_\eta^{eff} = (\eta/\mathcal{N}_q)\overline{d}^\dagger(\alpha_d c_d + \alpha_0 f_0 + \alpha_1 f_1)e^{-i\omega t} + \text{H. c.}, \quad (13)$$

where α_d, α_0, and α_1 depend on V, ε_d, U, and K.

The unperturbed effective Hamiltonian H_A^{eff} commutes with n_d. Of its eigenstates, only those with $n_d = 1$ are energetically accessible at the LM. It is safe to disregard the perturbation proportional to α_d in Eq. (13), which couples them to the subspaces $n_d = 0$ and $n_d = 2$.

The other two perturbations conserve n_d and are important even at very low energies. It is convenient to project them upon ϕ_0 and ϕ_1, because the spectral densities for f_0 and f_1 are phase-shift dependent. Substitution of Eq. (9) for $\alpha_0 f_0 + \alpha_1 f_1$ brings Eq. (13) to the form

$$H_\eta^{eff} = (\eta/\mathcal{N}_q)\overline{d}^\dagger(\beta_0\,\phi_0 + \beta_1\,\phi_1) + \text{H. c.}. \quad (14)$$

In the (LM to FL) crossover, just as the Kondo Hamiltonian $H_A^{eff} = e^S H_A e^{-S}$ is equivalent to H_A and the diagonalization of H_A^{eff} yields the physical properties for H_A, the effective perturbation H_η^{eff} is equivalent to H_η and application of the golden rule to H_η^{eff} yields the transition rate induced by H_η. Out of the terms then resulting from Eq. (14), only those proportional to $|\langle m|\phi_0^\dagger|n\rangle|^2$ and $|\langle m|\phi_1^\dagger|n\rangle|^2$ contribute to G_q [41]. The cross terms disregarded, the last two columns in Table 1 lead to

$$\langle j_{\,\overline{d}\to A}\rangle_T = \frac{\pi\eta^2}{\hbar}\left(\frac{\beta_0^2}{\mathcal{N}_q{}^2}\rho_0^S + \beta_1^2\,\rho_{SET}^S\right). \quad (15)$$

Comparison with Eq. (12) then shows that

$$\rho_q(\mathcal{E}, \mathcal{T}) = (\beta_0^2/\mathcal{N}_q{}^2)\rho_0^S(\mathcal{E}, \mathcal{T}) + \beta_1^2\,\rho_{SET}^S(\mathcal{E}, \mathcal{T}), \quad (16)$$

and Eq. (5) yields an expression for the conductance:

$$G_q(\mathcal{T}) = \beta_0^2\, G_0^S(\mathcal{T}) + \mathcal{N}_q{}^2 \beta_1^2\, G_{SET}^S(\mathcal{T}). \qquad (17)$$

Substitution of the expressions in the LM line of Table 2 for G_q, G_0^S, and G_{SET}^S shows that $\beta_0^2 = \sin^2\delta$, while the expressions in the FL line show that $\mathcal{N}_q{}^2\beta_1^2 = \cos^2\delta$. With this, Eq. (17) becomes

$$G_q(\mathcal{T}) = G_0^S(\mathcal{T})\, \sin^2\delta + G_{SET}^S(\mathcal{T})\, \cos^2\delta, \qquad (18)$$

and to complete the derivation of Eq. (1) we only have to recall that $G_0^S = \mathcal{G}_2 - G_{SET}^S$.

Table 3: Parameters for the five runs in Fig. 2b. $U = 0.20\,D$.

$-\varepsilon_d/D$	V/D	$-K/D$	q	δ/π	k_BT_K/D
0.10	3.6×10^{-4}	100.0	100	0.00	1.3×10^{-5}
0.17	0.021	0.315	1	0.22	1.1×10^{-5}
0.10	0.021	0.315	1	0.25	1.1×10^{-9}
0.022	0.021	0.315	1	0.28	1.1×10^{-5}
0.10	0.056	0.000	0	0.5	1.4×10^{-5}

Discussion. The phase shift δ and Kondo temperature T_K in Eq. (1) depend on the model parameters. Almost invariably, they have to be computed numerically, because the perturbative expressions for δ and T_K are accurate only in corners of the parametrical space [3, 17, 20, 26, 42]. Exceptions are the particle-hole symmetric Hamiltonians H_0^S [Eq. (2)] and H_{SET}^S [Eq. (4)], for which $\delta = \pi/2$ and $\delta = 0$, so that Eq. (1) reduces to $G_q(\mathcal{T}) = \mathcal{G}_2 - G_{SET}^S(\mathcal{T}) = G_0^S(\mathcal{T})$ and $G_q(\mathcal{T}) = G_{SET}^S(\mathcal{T})$, depicted in the right and left panels of Fig. 2b, respectively.

In other regions of the Kondo domain, δ lies between $-\pi/2$ and $\pi/2$. In the Kondo crossover, the conductance on the left-hand side of Eq. (1) changes by less than $\mathcal{G}_2$, from $\mathcal{G}_2 \sin^2\delta$ to $\mathcal{G}_2\cos^2\delta$. The rise or decay of $G_q(T)$ is centered at $\mathcal{G}_2/2$ and proportional to $G_{SET}^S - \mathcal{G}_2/2$.

The central panel of Fig 2b shows examples. The solid lines are Eq. (1) with δ (Table 3) extracted from the FL single-particle eigenvalues in the NRG diagonalization of the pertinent Hamiltonian H_A; and T_K (Table 3), from a fit of the universal magnetic susceptibility [18, 20] to the susceptibility computed for the same Hamiltonian. No adjustable parameter is therefore involved in the excellent agreement between Eq. (1) and the NRG data for the conductance. We have applied the same procedure to more than 100 NRG runs sampling the Kondo domain; in each one, the agreement was equally good.

In brief, the exact universal mapping (1) interpolates between $G(T \gg T_K)$ and $G(T \ll T_K)$. While the two extremes, described by single-particle Hamiltonians, are accessible to a variety of techniques—e. g., the Landauer-Buttiker formula or scattering-matrix analyses [43]—, the interpolation covers the temperature range beyond the reach of simple analyses.

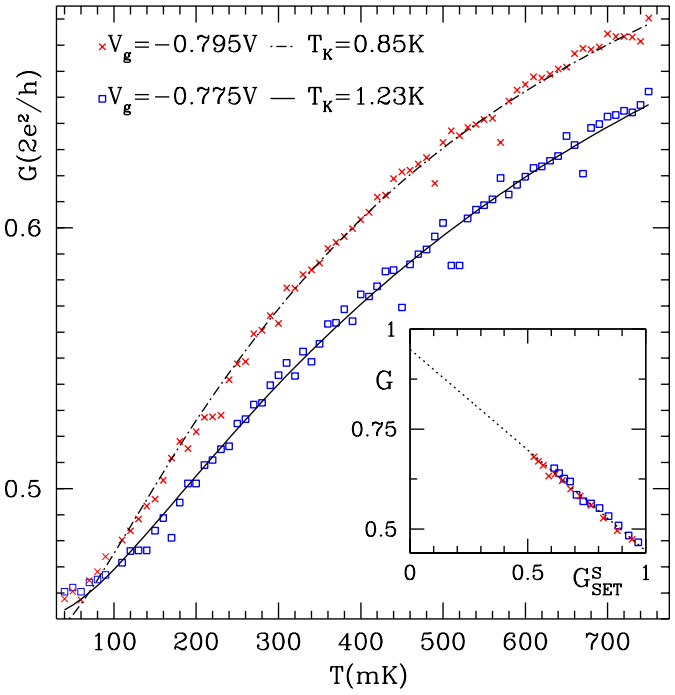

Figure 3: Comparison with experiment [8]. The crosses and squares are the conductances G at the indicated gate potentials V_g; the temperatures measured below 100mK carry large uncertainties [8]. The dash-dotted and solid lines depict Eq. (19). The inset shows that, for each V_g, the appropriate T_K straightens the plot of G vs. G_s and yields Eq. (19).

Comparison with experiment. To allow for the inevitable background currents, we exploit the linearity in Eq. (1). Given a set of N experimental pairs $\{G_i, T_i\}$, from a trial Kondo temperature T_K^* we generate the dimensionless temperatures $\mathcal{T}_i = T_i/T_K^*$ $(i = 1, \ldots, N)$. Next, we invert the function $G_s(\mathcal{T})$ to determine the universal conductance G_{si} for each $\mathcal{T}_i$. If the plot of G_i vs. G_{si} is straight, T_K^* is the Kondo temperature. If it is not, we iterate. Visual inspection (numerical evaluation of the curvature) determines T_K within 10% error (to an accuracy limited only by the experimental dispersion).

As an example, the inset of Fig. 3 treats the conductances in Fig. 3b of Ref. [8], measured with the gate potentials $V_g = -795\,\mathrm{mV}$ (squares) and $-775\,\mathrm{mV}$ (crosses), and yields the Kondo temperatures $T_K = 850\,\mathrm{mK}$ and 1230 mK, as well as the linear relation

$$G(\mathcal{T}) = 1.9e^2/h - 0.5G_{SET}^S(\mathcal{T}). \qquad (19)$$

For $T \gg T_K$, $G_{SET}^S(\mathcal{T}) \to 0$, so that $G \to 1.9e^2/h$, close to the measured off-resonance conductance $(1.8e^2/h)$ [8].

The agreement with the solid and the dash-dotted lines representing Eq. (19) in Fig. 3 shows that the data are in the Kondo regime and the contact resistance is negligible. There is, however, a background current: at $\mathcal{T} = 1$, Eq. (19) yields $G(\mathcal{T} = 1) = 1.4e^2/h$; the excess $G_b = 0.4e^2/h$ over $G(\mathcal{T}) = e^2/h$, predicted by Eq. (1) is the background conductance [8]. If we define

$\tilde{G} \equiv G - G_b$, then Eq. (19) takes the universal form $\tilde{G} - e^2/h = -0.5(G^S_{SET} - e^2/h)$, from which we find the shift: $\cos 2\delta = -0.5$ ($\delta \approx \pi/3$).

In conclusion, we have shown that, in the Kondo regime, measured from $\mathcal{G}_2/2$ and scaled by $\cos 2\delta$, the conductance of side-coupled devices is a universal function of T/T_K. Our application to experimental data identified inequivocally the measured thermal dependences with Kondo screening; detected a background current; and determined the ground-state phase shift.

* * *

We are grateful to Drs. Alvaro Ferraz, Vivaldo Campo, V. V. Ponomarenko, and R. Pepino for stimulating discussions; to Prof. Shingo Katsumoto for the data in Fig. 3. The CNPq, FAPESP (01/14974-0; 04/08928-3), and IBEM supported this work.

References

[1] Goldhaber-Gordon D., Shtrikman H., Mahalu D., Abusch-Magder D., Meirav U. and Kastner M. A., *Nature* , **391** (1998) 156.
[2] Goldhaber-Gordon D., Göres J., Kastner M. A., Shtrikman H., Mahalu D. and Meirav U., *Phys. Rev. Lett.* , **81** (1998) 5225.
[3] Hewson A. C., *The Kondo Problem to Heavy Fermions* (Cambridge University Press, Cambridge) 1993.
[4] Glazman L. I. and Raikh M. E., *JETP Lett.* , **47** (1987) 452.
[5] Costi T., Hewson A. and Zlatic V., *Journal of Physics–Condensed Matter* , **6** (1994) 2519.
[6] Bulla R., Costi T. and Pruschke T., *Rev. Mod. Phys.* , **80** (2008) 395.
[7] Kobayashi K., Aikawa H., Sano A., Katsumoto S. and Iye Y., *Phys. Rev. B* , **70** (2004) 035319.
[8] Sato M., Aikawa H., Kobayashi K., Katsumoto S. and Iye Y., *Phys. Rev. Lett.* , **95** (2005) 066801.
[9] Katsumoto S., Sato M., Aikawa H. and Iye Y., *Physica E: Low-dimensional Systems and Nanostructures* , **34** (2006) 36.
[10] Aharony A., Entin-Wohlman O., Otsuka T., Katsumoto S., Aikawa H. and Kobayashi K., *Phys. Rev. B* , **73** (2006) 195329.
[11] Fuhrer A., Brusheim P., Ihn T., Sigrist M., Ensslin K., Wegscheider W. and Bichler M., *Phys. Rev. B* , **73** (2006) 205326.
[12] Otsuka T., Abe E., Katsumoto S., Iye Y., Khym G. L. and Kang K., *J. Phys. Soc. Japan* , **76** (2007) 084706.
[13] Fano U., *Phys. Rev.* , **124** (1961) 1866.
[14] Hofstetter W., König J. and Schoeller H., *Phys. Rev. Lett.* , **87** (2001) 156803.
[15] Franco R., Figueira M. S. and Anda E. V., *Phys. Rev. B* , **67** (2003) 155301.
[16] Seridonio A. C., Yoshida M. and Oliveira L. N., arXiv:0906.4063 and arXiv:0906.4289.
[17] Wilson K. G., *Rev. Mod. Phys.* , **47** (1975) 773.
[18] Krishna-murthy H. R., Wilkins J. W. and Wilson K. G., *Phys. Rev. B* , **21** (1980) 1003.
[19] Oliveira L. N. and Wilkins J. W., *Phys. Rev. Lett.* , **47** (1981) 1553.
[20] Tsvelick A. M. and Wiegmann P. B., *Advances in Physics* , **32** (1983) 453.
[21] Lin C. L., Wallash A., Crow J. E., Mihalisin T. and Schlottmann P., *Phys. Rev. Lett.* , **58** (1987) 1232.
[22] Silva J. B., Lima W. L., Oliveira W. C., Mello J. L. N., Oliveira L. N. and Wilkins J. W., *Phys. Rev. Lett.* , **76** (1996) 275.
[23] van der Wiel W. G., Francheschi S. D., Fujisawa T., Elzerman J. M., Tarucha S. and Kouwenhoven L. P., *Science* , **289** (2000) 2105.
[24] Cronenwett S. M., Lynch H. J., Goldhaber-Gordon D., Kouwenhoven L. P., Marcus C. M., Hirose K., Wingreen N. S. and Umansky V., *Phys. Rev. Lett.* , **88** (2002) 226805.
[25] Liang W., Shores M. P., Bockrath M. and Long J. R., *Nature* , **417** (2002) 725.
[26] Krishna-murthy H. R., Wilkins J. W. and Wilson K. G., *Phys. Rev. B* , **21** (1980) 1044.
[27] Wingreen N. S. and Meir Y., *Phys. Rev. B* , **49** (1994) 11040.
[28] da Silva L. G. G. V. D., Sandler N. P., Ingersent K. and Ulloa S. E., *Phys. Rev. Lett.* , **97** (2006) 096603.
[29] Maruyama I., Shibata N. and Ueda K., *J. Phys. Soc. Japan* , **73** (2004) 3239.
[30] Torio M. E., Hallberg K., Ceccatto A. H. and Proetto C. R., *Phys. Rev. B* , **65** (2002) 085302.
[31] Zitko R. and Bonca J., *Phys. Rev. B* , **73** (2006) 035332.
[32] Bulka B. R., Tolea M. and Dinu I. V., *Phys. Rev. B* , **74** (2006) 205301.
[33] Seridonio A. C., Souza F. M. and Shelykh I. A., *J. Phys. Cond. Matter* , **21** (2009) 095003 compare the SET and side-coupled devices to a STM near a Kondo impurity.
[34] Given the inversion symmetry of Fig. 1, we define conduction states c_k (b_k) with even (odd) parity. Decoupled from the dot, the b_k's need not appear in H_A.
[35] Neither our analysis nor its result [Eq (1)] depend on the number of terms in the expansion of V_k.
[36] At low energies ($\tilde{\epsilon}_p \ll D$), $\alpha_{pk} = \Delta/\pi(\tilde{\epsilon}_p - \epsilon_k)$.
[37] Greenwood D. A., *Proc. Phys. Soc., London* , **71** (1958) 585.
[38] Langreth D. C., *Phys. Rev.* , **150** (1966) 516.
[39] Schrieffer J. R. and Wolff P. A., *Phys. Rev.* , **149** (1966) 491.
[40] Projected on the $\{g_k\}$ basis, H_A^{eff}/k_BT_K has universal eigenvalues and eigenvectors. Thermally averaged expectation values involving only the operators $\phi_0 \sim \sum_k g_k$ and $\phi_1 \sim \sum_k \varepsilon_k g_k$ are therefore universal functions.
[41] The contribution to ρ_q of the cross terms, $\rho_{01}(\epsilon) \equiv \sum_{mn} e^{-\beta E_m}/f(\epsilon)\langle m|\phi_0^\dagger|n\rangle\langle n|\phi_1|m\rangle\delta(\epsilon - \epsilon_{mn}) + c.\ c.$, is universal [40]. We can therefore choose $H_A = H_0^S$ to compute it. Given that H_0^S is invariant under particle-hole transformations, while $\rho_{01}(\epsilon) \to -\rho_{01}(-\epsilon)$, we see that $\rho_{01}(\epsilon)$ is an odd function of the energy; substituted for $\rho_q(\epsilon)$ in Eq. (5), it makes no contribution to G_q.
[42] Andrei N., Furuya K. and Lowenstein J. H., *Rev. Mod. Phys.* , **55** (1983) 331.
[43] Büttiker M., *Phys. Rev. Lett.* , **57** (1986) 1761.